

# Control Design for Optimizing Efficiency in Inductive Power Transfer Systems

Zhichong Huang, *Student Member, IEEE*, Siu-Chung Wong, *Senior Member, IEEE*, and Chi K. Tse, *Fellow, IEEE*

**Abstract**—Inductive power transfer (IPT) converters are resonant converters that attain optimal energy efficiencies for a certain load range. To achieve maximum efficiency, it is common to cascade the IPT converter with front-side and load-side dc/dc converters. The two dc/dc converters are normally controlled cooperatively for the requirements of output regulation and maximum efficiency tracking using a control technique based on perturbation and observation, which is inevitably slow in response. In this paper, a decoupled control technique is developed. The load-side dc/dc converter is solely responsible for output regulation while the front-side converter is responsible for impedance-matching of the IPT converter by controlling its input-to-output voltage ratio. The controls are linear and therefore fast. DC and small-signal transfer functions are derived for designing the control parameters. The performances of fast regulation and high efficiency of the IPT converter system are verified using a prototype system.

**Index Terms**—Inductive power transfer, wireless power transfer, control for maximum efficiency.

## I. INTRODUCTION

Design and optimization of inductive power transfer (IPT) systems have been widely studied. One of the main objectives is to achieve high efficiency. The optimization involves the choice of appropriate structure of magnetic couplers [1] and their interoperability [2]. It is well known that a higher coupling coefficient and higher coil quality factors of the pair of windings of the magnetic coupler would increase the system efficiency [3], [4]. Optimization approaches for these two parameters to achieve high efficiency have been proposed [5], [6]. Meanwhile, since the system efficiency is not monotonically varying with the load, optimum loads that achieve maximum efficiency of the system are also studied [7]–[9]. Moreover, various design aspects to achieve maximum efficiency for different converter input-output transfer functions using series and parallel compensations have been studied [10], [11]. Previous studies show that given a coupling coefficient and coil quality factors, an IPT converter should be designed to operate at some fixed operating frequencies with load-independent transfer characteristic and slight modulation for soft switching when a simple half-bridge or full-bridge inverter circuit is used, and to operate within a restricted

load range in order to achieve maximum efficiency [10]–[13]. Among the four basic types of compensation, the widely used *series-series* compensated IPT (SSIPT) converter is the most power efficient IPT converter when it is operating with load-independent output current [7]–[13]. However, in some practical applications, the design may not meet the required wide variations of the coupling coefficient, the load resistance and the load power. Thus, once an IPT converter has been designed at a particular coupling coefficient and a particular load, the efficiency of the IPT system cannot always be maintained near its maximum point.

To improve the system efficiency under variation of the load, a load-side dc/dc converter is connected between the load and the secondary of an SSIPT converter to adaptively control the equivalent load observed by the SSIPT converter, thus maintaining a maximum efficiency of the front-end power amplifier driver [14], [15]. To achieve output regulation, source modulation is needed. The modulation can be provided by either a pulse-width modulated inverter, a front-side dc/dc converter which amplitude-modulates the inverter circuit, or a power amplifier. The inverter circuit is mostly implemented by either a half-bridge or full-bridge circuit which provides the highest efficiency but suffers from shallow modulation due to the need for maintaining soft switching [9]–[11]. The depth of modulation can be greatly improved when the inverter is amplitude-modulated by a front-end dc/dc converter. The combined circuit incurs a penalty of additional loss due to the extra power stage. The power amplifier can be considered as a circuit consisting of a front-side dc/dc converter, amplitude modulating an inverter circuit with an output filter. The study by Li *et al.* [16] shows that a system consisting of an SSIPT converter with front-side and load-side dc/dc converters (the system is denoted as F-SSIPT-L) can achieve better overall system efficiency compared to a system consisting of the same SSIPT converter and a load-side dc/dc converter utilizing the modulation of the internal inverter (such a system is denoted as M-SSIPT-L) with frequency modulation. A maximum efficiency tracking (MET) algorithm has been proposed by Li *et al.* [16], where the secondary dc/dc converter regulates the output voltage while the front-side dc/dc converter maximizes the system efficiency. Another MET algorithm has also been studied using the F-SSIPT-L system where the front-side dc/dc converter controls the input current of the SSIPT converter for better handling of small coupling coefficient and light load [17]. Furthermore, a MET algorithm has been applied to the inverter to minimize the input power of an M-SSIPT-L system

Manuscript received Dec. 9, 2016; revised April 3, 2017; accepted June 27, 2017.

This work is supported by Hong Kong Polytechnic University under Central Research Grant G-YBKC.

The authors are with the Department of Electronic and Information Engineering, The Hong Kong Polytechnic University, Kowloon, Hong Kong (Email: zhichong.huang@connect.polyu.hk; enschwong@polyu.edu.hk; enck-tse@polyu.edu.hk)

0000-0000/00\$00.00 © 2017 IEEE

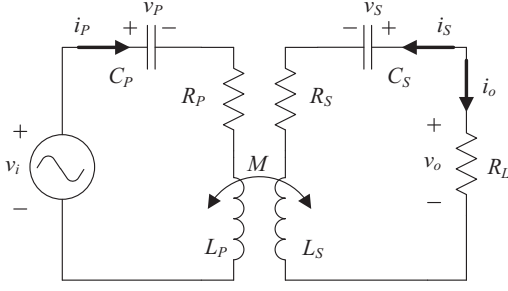


Fig. 1. IPT converter model.

where the load-side dc/dc converter solely regulates the output [18]. The benefit is that no wireless data feedback is needed from the secondary to the primary of the magnetic coupler. The MET control schemes studied so far are based on perturbation and observation (P&O) of the system power or the system efficiency [15]–[18]. It is well known that P&O based control schemes are slow due to the uncertainties of perturbation speed and amplitude. Moreover, such control schemes are based on real-time processing of both voltage and current for obtaining information of power or efficiency, resulting in high error of the processed information and necessitating the use of cost-ineffective current sensor(s). In this paper, a simple and fast voltage control scheme for achieving maximum efficiency of the SSIPT converter is proposed for applications requiring fast regulation of load powers, such as charging of electric vehicles [29]–[31] and biomedical implants [32], [33].

## II. MAXIMUM IPT CONVERTER EFFICIENCY AND VOLTAGE RATIO

Fig. 1 shows an equivalent circuit of a commonly used SSIPT converter model, where the magnetic coupler has self inductances  $L_P$  and  $L_S$ , and mutual inductance  $M$ . The magnetic coupler is compensated by external series compensated capacitors  $C_P$  and  $C_S$ . Subscripts  $P$  and  $S$  indicate parameters on the primary and secondary sides, respectively, of the magnetic coupler. The circuit is simplified as being driven by an approximate equivalent ac voltage source  $v_i$  at a fundamental angular frequency  $\omega$  modulated by the inverter. The output is usually rectified to drive a dc load with  $R_L$  being the ac equivalent resistance. Losses are modeled aggregately using equivalent series resistors  $R_P$  and  $R_S$  [10]. Resistor  $R_P$  includes losses from the primary windings and the inverter circuit while resistor  $R_S$  includes losses from the secondary windings and the rectifier circuit.

This SSIPT model has been studied in refs. [9]–[11] with converter efficiency  $\eta$  and transconductance  $G$  given as

$$\eta(\omega, R_L) = \frac{\omega^2 M^2 R_L}{|Z_S + R_L|^2 R_P + \omega^2 M^2 (R_S + R_L)}, \text{ and } (1)$$

$$G(\omega) = \frac{i_o}{v_i} = \frac{j\omega M}{Z_P(Z_S + R_L) + \omega^2 M^2}. \quad (2)$$

where  $Z_P = j\omega L_P + \frac{1}{j\omega C_P} + R_P$  and  $Z_S = j\omega L_S + \frac{1}{j\omega C_S} + R_S$  are the impedance of the primary resonator and the secondary resonator, respectively.

For simplicity, the SSIPT converter is normally designed to operate at the aligned resonant frequency, i.e.,  $\omega = \omega_P = \omega_S$ , where  $\omega_P = \frac{1}{\sqrt{L_P C_P}}$  and  $\omega_S = \frac{1}{\sqrt{L_S C_S}}$  [9], [18]. As a result,  $\eta$  in (1) is maximized at a particular load  $R_{L,\text{opt}}$  which can be calculated by solving  $\frac{\partial \eta}{\partial R_L} = 0$ , i.e.,

$$R_{L,\text{opt}} = R_S \sqrt{1 + \frac{\omega^2 M^2}{R_P R_S}} \quad (3)$$

$$\approx \omega M \sqrt{\frac{R_S}{R_P}} \text{ for } \frac{\omega^2 M^2}{R_P R_S} \gg 1. \quad (4)$$

The magnitude of the transconductance  $|G|$  at this operating frequency is given by

$$|G| = \left| \frac{i_o}{v_i} \right| = \frac{\omega M}{R_P(R_S + R_L) + \omega^2 M^2}. \quad (5)$$

for  $\frac{\omega^2 M^2}{R_P R_S} \gg 1$  and  $\frac{\omega^2 M^2}{R_P R_L} \gg 1$ .

The magnitude of the voltage transfer ratio  $|H|$  at maximum efficiency is thus given by

$$|H| = \left| \frac{v_o}{v_i} \right| = |G| R_{L,\text{opt}} \approx \sqrt{\frac{R_S}{R_P}}. \quad (6)$$

From (6), it is possible to maintain a high IPT converter efficiency by controlling the converter voltage ratio at  $|H| = \sqrt{\frac{R_S}{R_P}}$  against variation of the load.

## III. SSIPT CONVERTER VOLTAGE RATIO CONTROL

A general three-stage IPT system is shown in Fig. 2 [16]–[18]. The IPT system includes a front-side dc/dc converter, an SSIPT converter and a load-side dc/dc converter. The operating frequency of the inverter is fixed at the resonant frequency to achieve maximum efficiency. The control functions of the three-stage system provide

- 1) regulation to the output voltage or current, and
- 2) control for maximum efficiency of the SSIPT converter.

Three control schemes with control functions  $V_{\text{err}}(m_1)$ ,  $\eta(m_1)$  and  $P_{\text{IN}}(m_1)$  are shown in Fig. 2 and compared in Table I, where  $m_1$  is a modulation index of  $V_{\text{IN}}$ . The following advantages of our proposed linear control method can be readily observed:

- 1) The control function versus modulated index  $m_1$  (e.g. duty cycle of the front-side converter) is monotonic with a well defined control reference  $V_{\text{err}} = 0$  to minimize error voltage  $V_{\text{err}} = V_1 - \sqrt{\frac{R_P}{R_S}} V_2$ , i.e., to achieve the desired  $|H|$  in (6). With a proper design, a simple linear PI controller can be implemented in either analog or digital form. This results in a faster response.
- 2) The sampled voltages can be used for the linear PI controller without further processing. This results in a faster and more accurate response. Moreover, no current sensor is required, and the system cost is lower.

The steady-state operation of the converter system is studied in this section. Small-signal analysis will be conducted in Section IV. The load-side converter regulates the output voltage or current so that the load appears as a power load  $P_O$  at the output of the SSIPT converter. Power balance requires

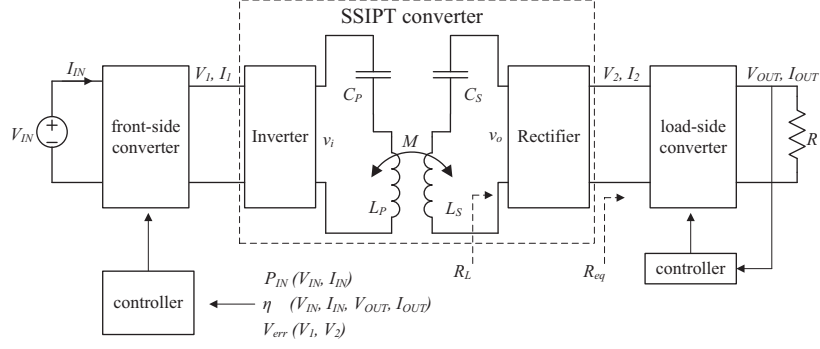


Fig. 2. An SSIPT converter cascaded with a front-side converter and a load-side converter.

TABLE I  
COMPARISON OF DIFFERENT CONTROL SCHEMES

Control function	$V_{err}$ , voltage error control (this paper)	$\eta$ , maximum efficiency tracking [16], [17]	$P_{IN}$ , minimum input power tracking [18]
Monotonicity	$\frac{\Delta V_{err}}{\Delta m_1}$ is always positive	probing $\frac{\Delta \eta}{\Delta m_1}$ for signs	probing $\frac{\Delta P_{in}}{\Delta m_1}$ for signs
Control reference	$V_{err,ref} = 0$	adaptively tracking the maximum point.	adaptively tracking the minimum point.
Control method	PI controller, analog or digital	P&O, digital	P&O, digital
Sampling	$V_1, V_2$	$V_{IN}, I_{IN}, V_{OUT}, I_{OUT}$	$V_{IN}, I_{IN}$

that  $P_O = V_2 I_2$ . Substituting (5) and applying a scaling factor between square and sinusoidal magnitudes, we have  $\frac{1}{\omega M} = \left| \frac{i_o}{v_i} \right| = \frac{\pi}{4} \frac{I_2}{V_1}$ , which gives

$$P_O = V_2 \frac{8}{\pi^2 \omega M} V_1. \quad (7)$$

To achieve (6), it is equivalent to minimize  $|V_{err}|$  given by

$$V_{err} = V_1 - \sqrt{\frac{R_P}{R_S}} V_2 = V_1 - \sqrt{\frac{R_P}{R_S}} \frac{P_O \pi^2 \omega M}{8} \frac{1}{V_1}. \quad (8)$$

When using a front-side PWM converter,  $V_1$  is the modulated output of  $V_{IN}$  from modulation index  $m_1 = \frac{V_1}{V_{IN}}$ . Monotonic curves for the control function  $V_{err}$  of (8) are shown in Table I for various values of coupling coefficient  $k = \frac{M}{\sqrt{L_P L_S}}$ . A linear PI controller can be used for its simple structure, better robustness and high reliability. The design will be presented in Section IV.

#### IV. CONTROLLER DESIGN

Linear PI controllers will be designed to optimize the efficiency of the SSIPT converter system. Fig. 3 shows a proposed schematic of control for the system. For the SSIPT converter, an H-bridge inverter is used to generate an ac voltage at the resonant frequency. Thus, the SSIPT converter behaves

as a transconductance converter [11]. The current output is cascaded with a buck-boost converter which is regulated with a stand-alone PI controller to generate a constant voltage output  $V_{OUT}$ . The front-side converter is a buck converter whose output voltage  $V_1$  drives the SSIPT converter. Voltages  $V_1$  and  $V_2$  of the SSIPT converter are sampled. No current sensor is needed here. Voltage  $V_2$  after being scaled by a factor of  $\sqrt{\frac{R_P}{R_S}}$  is transmitted wirelessly from the secondary to the primary of the magnetic coupler and connected to the input of the PI controller of the buck converter. The voltage error  $V_{err}$  is nulled by the PI controller of the buck converter to achieve maximum efficiency of the SSIPT converter.

At the optimal efficiency point, steady-state parameters of the converters are calculated using  $R_{eq} = \frac{\pi^2}{8} \omega M \sqrt{\frac{R_S}{R_P}}$ ,  $R_{buck} = \frac{\pi^2}{8} \omega M \sqrt{\frac{R_P}{R_S}}$ ,  $V_2 = V_{OUT} \sqrt{\frac{R_{eq}}{R}}$ , and  $V_1 = V_{OUT} \sqrt{\frac{R_{buck}}{R}}$ . For simplicity, the front-side and load-side converters are assumed lossless.

##### A. SSIPT Model

The small-signal transfer function of the SSIPT converter can be derived and calculated using the *generalized averaging*

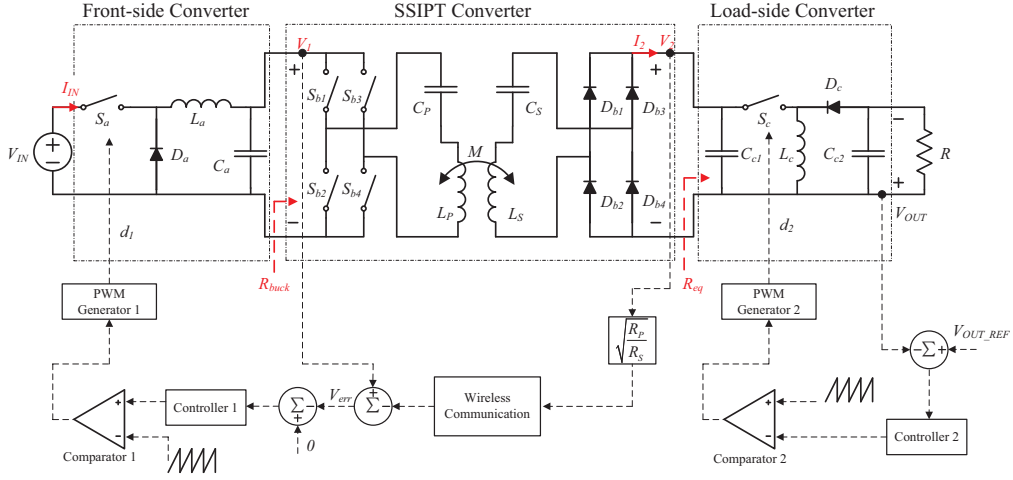


Fig. 3. Schematic of the system.

technique given in [19], [20] for ordinary PWM and resonant power converters. Later, the same technique has been rephrased as *dynamic-phasor model* and applied for single-phase induction machines [21], microgrid systems [27] and extended for the predictive control of power converters [28]. Since the application of the generalized averaging technique or the dynamic-phasor model may not be obvious for IPT converters, the procedure is highlighted as follows. A sinusoidal signal  $x(t)$  with time-varying magnitude  $X$  and phase angle  $\theta$  can be written by

$$x(t) = X \sin(\omega t + \theta) \quad (9)$$

$$= X [\cos \theta \sin \omega t + \sin \theta \cos \omega t] \quad (10)$$

$$= X_d \sin \omega t + X_q \cos \omega t \quad (11)$$

$$= \Im((X_d + jX_q)e^{j\omega t}), \quad (12)$$

where  $X_d = X \cos \theta$ ,  $X_q = X \sin \theta$  are the direct and quadrature components of  $x(t)$ . The time functions of the slow time-varying properties of  $X$ ,  $\theta$ ,  $X_d$  and  $X_q$  are omitted for brevity. It can be readily shown that

$$\frac{dx(t)}{dt} = \Im \left\{ \left[ \left( \frac{dX_d}{dt} - \omega X_q \right) + j \left( \frac{dX_q}{dt} + \omega X_d \right) \right] e^{j\omega t} \right\}. \quad (13)$$

For a pure capacitor  $C$  having current  $i_C(t)$  and voltage  $v_C(t)$ , and a pure inductor  $L$  having current  $i_L(t)$  and voltage  $v_L(t)$ , the following basic relationships hold

$$i_C(t) = C \frac{dv_C(t)}{dt}, \text{ and} \quad (14)$$

$$v_L(t) = L \frac{di_L(t)}{dt}. \quad (15)$$

Substituting (12) and (13) into (14) and (15) and simplifying, we have

$$I_{C,d} + jI_{C,q} = C \left( \frac{dV_{C,d}}{dt} - \omega V_{C,q} \right) + j \left( \frac{dV_{C,q}}{dt} + \omega V_{C,d} \right), \text{ and} \quad (16)$$

$$V_{L,d} + jV_{L,q} = L \left( \frac{dI_{L,d}}{dt} - \omega I_{L,q} \right) + j \left( \frac{dI_{L,q}}{dt} + \omega I_{L,d} \right). \quad (17)$$

We can write  $x(t)$  as a complex vector given as  $\dot{X} = X_d + jX_q$ . Hence, (16) and (17) can be simplified at steady-state to become

$$\dot{I}_C = I_{C,d} + jI_{C,q} = j\omega \dot{V}_C, \text{ and} \quad (18)$$

$$\dot{V}_L = V_{L,d} + jV_{L,q} = j\omega \dot{I}_L, \quad (19)$$

which is commonly used in complex vector analysis. Obviously, (16) and (17) are vector transformations of (14) and (15). We can write (16) and (17) in matrix forms as

$$\mathbf{I}_C = C \left( \mathbb{I}_\omega + \frac{d}{dt} \right) \mathbf{V}_C, \text{ and} \quad (20)$$

$$\mathbf{V}_L = L \left( \mathbb{I}_\omega + \frac{d}{dt} \right) \mathbf{I}_L, \quad (21)$$

where  $\mathbf{X}_Y = [X_{Y,d}, X_{Y,q}]^T$  is a column vector and

$$\mathbb{I}_\omega = \begin{pmatrix} 0 & -\omega \\ \omega & 0 \end{pmatrix} \quad (22)$$

is a  $2 \times 2$  matrix.

The SS IPT system shown in Fig. 1 is governed by a state-space equation given as

$$\frac{d}{dt} \mathbf{X} = \mathbf{A} \mathbf{X} + \mathbf{B} \mathbf{V}, \quad (23)$$

where

$$\mathbf{X} = \begin{bmatrix} v_P(t) & v_S(t) & i_P(t) & i_S(t) \end{bmatrix}^T \quad (24)$$

$$\mathbf{V} = \begin{bmatrix} v_i(t) & v_o(t) \end{bmatrix}^T \quad (25)$$

$$\mathbf{A} = \begin{bmatrix} 0 & 0 & \frac{1}{C_P} & 0 \\ 0 & 0 & 0 & \frac{1}{C_S} \\ -\alpha_P & \beta & -\alpha_P R_P & \beta R_S \\ \beta & -\alpha_S & \beta R_P & -\alpha_S R_S \end{bmatrix} \quad (26)$$

$$\mathbf{B} = \begin{bmatrix} 0 & 0 & \alpha_P & -\beta \\ 0 & 0 & -\beta & \alpha_S \end{bmatrix}^T \quad (27)$$

$$\alpha_P = \frac{1}{L_P(1-k^2)}, \quad (28)$$

$$\alpha_S = \frac{1}{L_S(1-k^2)}, \quad (29)$$

$$\beta = \frac{k}{(1-k^2)\sqrt{L_P L_S}}, \quad (30)$$

$v_P(t)$  is the voltage of  $C_P$ ,  $v_S(t)$  is the voltage of  $C_S$ ,  $i_P(t)$  is the current of  $L_P$  and  $i_S(t)$  is the current of  $L_S$ . The SSIPT system has input  $v_i(t)$  and output  $v_o(t)$  powering load  $R_L$ . All state variables are sinusoidal.

Equation (23) can be readily vector transformed using (20) and (21) to obtain

$$\frac{d}{dt}\mathbf{X} = \mathbf{A}\mathbf{X} + \mathbf{B}\mathbf{V}, \quad (31)$$

where

$$\mathbf{X} = \begin{bmatrix} \mathbf{V}_P & \mathbf{V}_S & \mathbf{I}_P & \mathbf{I}_S \end{bmatrix}^T \quad (32)$$

$$\mathbf{V} = \begin{bmatrix} \mathbf{V}_I & \mathbf{V}_O \end{bmatrix}^T \quad (33)$$

$$\mathbf{A} = \begin{bmatrix} -\mathbb{I}_\omega & 0 & \frac{1}{C_P}\mathbb{I}_2 & 0 \\ 0 & -\mathbb{I}_\omega & 0 & \frac{1}{C_S}\mathbb{I}_2 \\ -\alpha_P\mathbb{I}_2 & \beta\mathbb{I}_2 & -\alpha_P R_P\mathbb{I}_2 - \mathbb{I}_\omega & \beta R_S\mathbb{I}_2 \\ \beta\mathbb{I}_2 & -\alpha_S\mathbb{I}_2 & \beta R_P\mathbb{I}_2 & -\alpha_S R_S\mathbb{I}_2 - \mathbb{I}_\omega \end{bmatrix} \quad (34)$$

$$\mathbf{B} = \begin{bmatrix} 0 & 0 & \alpha_P\mathbb{I}_2 & -\beta\mathbb{I}_2 \\ 0 & 0 & -\beta\mathbb{I}_2 & \alpha_S\mathbb{I}_2 \end{bmatrix}^T \quad (35)$$

$\mathbb{I}_2$  is the 2-dimensional identity matrix and variable  $\mathbf{X}_Y = (X_{Yr}, X_{Yi})^T$ .

A converter is cascaded with the SSIPT instead of a resistor. Assumed that the converter is well controlled to maintain a constant voltage or current output, it can be considered as a constant power load [22]. The extended describing function of  $\mathbf{V}_O$  is given by

$$V_{O,d} = -2P_O \frac{I_{S,d}}{I_{S,d}^2 + I_{S,q}^2}, \quad (36)$$

$$V_{O,q} = -2P_O \frac{I_{S,q}}{I_{S,d}^2 + I_{S,q}^2}, \quad (37)$$

where  $P_O$  is the output power of the SSIPT. With (31), (36) and (37), the small-signal model of (31) can be derived as

$$\begin{cases} \frac{d}{dt}\hat{\mathbf{X}} = \hat{\mathbf{A}}\hat{\mathbf{X}} + \hat{\mathbf{B}}\hat{\mathbf{V}}_I \\ \hat{\mathbf{I}}_O = \hat{\mathbf{C}}\hat{\mathbf{X}} \end{cases} \quad (38)$$

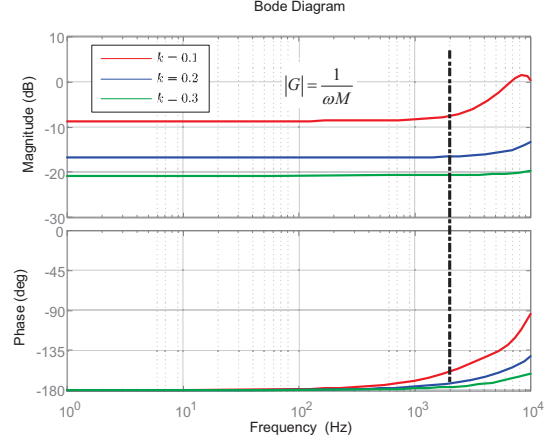


Fig. 4. Simulated frequency response of transconductance of the SSIPT model. Parameters used in simulation are:  $L_P = L_S = 30 \mu\text{H}$ ,  $C_P = C_S = 21.11 \text{ nF}$ ,  $R_P = R_S = 0.5 \Omega$ ,  $\frac{\omega}{2\pi} = 200 \text{ kHz}$ ,  $v_i = 30 \text{ V}$  and  $P_O = 60 \text{ W}$ .

where

$$\hat{\mathbf{X}} = \begin{bmatrix} \hat{\mathbf{V}}_P & \hat{\mathbf{V}}_S & \hat{\mathbf{I}}_P & \hat{\mathbf{I}}_S \end{bmatrix}^T, \quad (39)$$

$$\hat{\mathbf{V}}_I = \begin{bmatrix} \hat{\mathbf{V}}_{I,d} & \hat{\mathbf{V}}_{I,q} \end{bmatrix}^T, \quad (40)$$

$$\hat{\mathbf{I}}_O = \begin{bmatrix} \hat{\mathbf{I}}_{O,d} & \hat{\mathbf{I}}_{O,q} \end{bmatrix}^T, \quad (41)$$

$$\hat{\mathbf{A}} = \begin{bmatrix} -\mathbb{I}_\omega & 0 & \frac{1}{C_P}\mathbb{I}_2 & 0 \\ 0 & -\mathbb{I}_\omega & 0 & \frac{1}{C_S}\mathbb{I}_2 \\ -\alpha_P\mathbb{I}_2 & \beta\mathbb{I}_2 & -\alpha_P R_P\mathbb{I}_2 - \mathbb{I}_\omega & \beta(R_S\mathbb{I}_2 + \mathbb{I}_\delta) \\ \beta\mathbb{I}_2 & -\alpha_S\mathbb{I}_2 & \beta R_P\mathbb{I}_2 & -\alpha_S(R_S\mathbb{I}_2 + \mathbb{I}_\delta) - \mathbb{I}_\omega \end{bmatrix}, \quad (42)$$

$$\hat{\mathbf{B}} = \begin{bmatrix} 0 & 0 & \alpha_P\mathbb{I}_2 & -\beta\mathbb{I}_2 \end{bmatrix}^T, \quad (43)$$

$$\hat{\mathbf{C}} = \begin{bmatrix} 0 & 0 & 0 & -\mathbb{I}_\omega \end{bmatrix}, \quad (44)$$

$$\mathbb{I}_\delta = \begin{pmatrix} P & -P \\ P & -P \end{pmatrix}, \text{ and} \quad (45)$$

$$P = 2P_O \frac{-i_{S,d}^2 + i_{S,q}^2}{(i_{S,d}^2 + i_{S,q}^2)^2}. \quad (46)$$

The frequency response of the transconductance of the SSIPT converter is plotted using Matlab with details shown in Fig. 4. We observe that, within a bandwidth of one-hundredth of the fundamental frequency, the simulated transconductance can be approximated as an ideal transconductance  $\frac{1}{\omega M}$ , which is load independent.

### B. Voltage Error Control Loop

We define  $\hat{x}_y$  as the small-signal variable of  $X_y$ . Since the designed bandwidth of the control will be far lower than one-hundredth of the fundamental frequency, the SSIPT converter in Fig. 3 will be considered as a constant transconductance, given by

$$G_I = \frac{\hat{i}_2}{\hat{v}_1} = \frac{8}{\pi^2} \frac{1}{\omega M}. \quad (47)$$

General wireless communication protocols, like 2.4G, are fast enough to transmit the output voltage  $V_2$  of the SSIPT



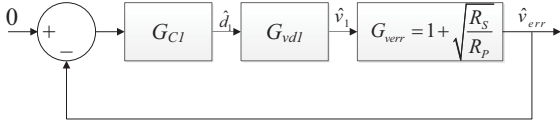


Fig. 5. Block diagram of the voltage control loop of the cascaded buck-SSIPT converter system.

converter, and the time delay is not considered here [3]. The load-side buck-boost converter is assumed to be ideally controlled as a constant power load, its small-signal input impedance is considered as a negative resistance  $-R_{eq}$  in this small signal model [22]. Voltage  $\hat{v}_2$  is thus given as

$$\hat{v}_2 = \hat{v}_1 G_I(-R_{eq}) = -\hat{v}_1 \sqrt{\frac{R_S}{R_P}}. \quad (48)$$

From (6) and the bandwidth considered, the voltage error transfer function of the SS IPT converter is assumed as

$$G_{v_{err}} = \frac{\hat{v}_1 - \hat{v}_2}{\hat{v}_1} = 1 + \sqrt{\frac{R_S}{R_P}}. \quad (49)$$

The input voltage  $\hat{v}_1$  of the SS IPT converter is controlled by the front-side buck converter shown in Fig. 3, the control-to-output transfer function of the buck converter is given by [23]

$$G_{vd1} = \frac{\hat{v}_1}{\hat{d}_1} = \frac{V_{IN}}{L_a C_a s^2 + \frac{L_a}{R_{buck}} s + 1}. \quad (50)$$

The control loop of the system is shown in Fig. 5. The transfer function of the input duty cycle  $\hat{d}_1$  to the voltage error  $\hat{v}_{err}$  is given by  $G_{vd1} G_{v_{err}}$ , of which the Bode diagram is shown in Fig. 6(a). For this system, the design of the compensator  $G_{C1}$  is similar to that of a buck converter [24]. Thus, a simple PI controller  $G_{C1}$  can be chosen as

$$G_{C1} = \frac{K_P s + K_I}{s}. \quad (51)$$

### C. Stability Analysis

The open loop transfer function  $T$  of the front-side buck converter cascaded with the SS IPT converter (buck-SS IPT converter) is given by

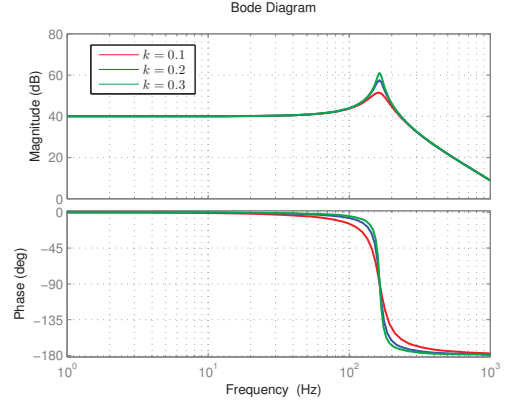
$$T = G_{C1} G_{vd1} G_{v_{err}}. \quad (52)$$

By substituting (49), (50), (51) into (52) and putting  $1 + T = 0$ , a third-order characteristic equation of the buck-SS IPT converter is obtained as

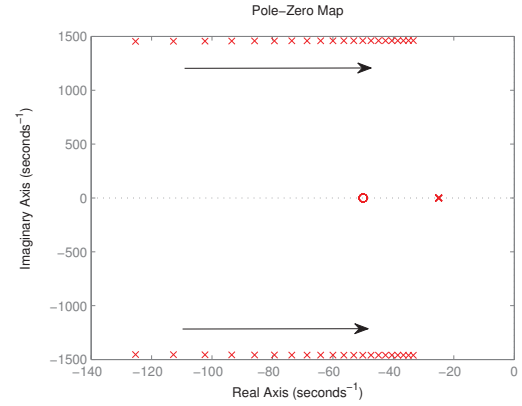
$$a_3 s^3 + a_2 s^2 + a_1 s + a_0 = 0, \quad (53)$$

where  $a_3 = L_a C_a$ ,  $a_2 = \frac{L_a}{R_{buck}}$ ,  $a_1 = (1 + \sqrt{\frac{R_S}{R_P}}) K_P V_{IN} + 1$  and  $a_0 = (1 + \sqrt{\frac{R_S}{R_P}}) K_I V_{IN}$ .

The load  $R$  and the coupling coefficient  $k$  usually vary within some ranges during operation. For stable control,  $K_P$  and  $K_I$  should be designed to ensure system stability for the whole operating range. From the characteristic equation,  $R$  does not contribute to the design of  $K_P$  and  $K_I$ . An example design of the controller shown in Fig. 6(b) illustrates that all roots locate on the left-half-plane. Therefore, the stability of the system is ensured for  $k$  varying from 0.1 to 0.3.



(a) Frequency response of  $\hat{v}_{err}$  versus  $\hat{d}_1$ .



(b) Locations of pole (marked with 'x') and zero (marked with 'o') of the buck-SS IPT converter with  $K_P = 0.01$ ,  $K_I = 0.5$ , when  $k$  increases from 0.1 to 0.3 as indicated by the arrow direction.

Fig. 6. Small-signal characteristics of the buck-SS IPT converter. Simulation parameters of the SS IPT converter are  $L_P = L_S = 30 \mu\text{H}$ ,  $C_P = C_S = 21.11 \text{ nF}$ , and  $\frac{\omega}{2\pi} = \frac{\omega_P}{2\pi} = \frac{\omega_S}{2\pi} = 200 \text{ kHz}$ . Parameters of the buck converter are  $L_a = 1.2 \text{ mH}$ ,  $C_a = 760 \mu\text{F}$ ,  $V_{IN} = 50 \text{ V}$ ,  $V_O = 30 \text{ V}$ , and  $R = 20 \Omega$ .

## V. EXPERIMENTAL VERIFICATION

An experimental prototype as shown in Fig. 7 is built to verify the linear control scheme and a version of P&O control scheme [18] is also implemented for comparison. The parameters of the schematic shown in Fig. 3 are given in Table II.

### A. Design of Control Parameters

When the magnetic coupler is designed without a magnetic core, the variation of the air gap distance has little effect on the self inductances. Thus, the resonant frequency can be considered as constant and the operating frequency of the inverter can be fixed. However, when the magnetic coupler is designed with a magnetic core to improve the coupling coefficient, the variation of the air gap distance will affect the self inductances significantly [25]. Therefore, the operating frequency of the inverter should be dynamically adjusted to match the resonant frequency by using additional control, such as the self-oscillating control given in [26]. For the prototype

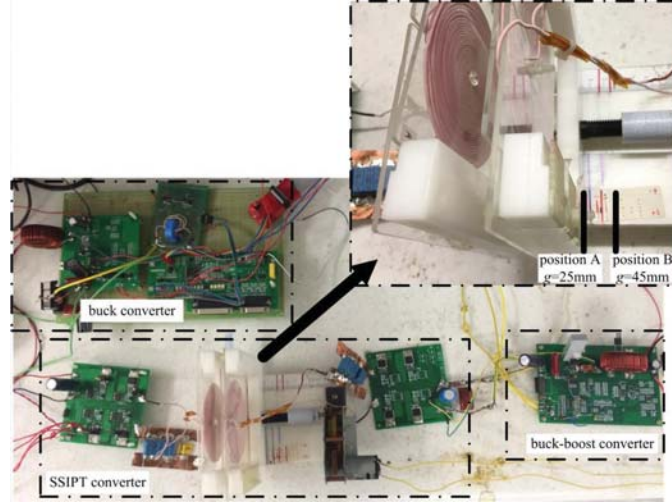


Fig. 7. Experiment setup of the system and enlarged image of the loosely coupled transformer.

TABLE II  
COMPONENTS AND PARAMETERS OF THE SYSTEM

Converter	Parameters	Symbol	Value		
Buck	Switch	$S_a$	IRF540N		
	Diode	$D_a$	MBR20100CTG		
	Inductor	$L_a$	1.2 mH		
	Capacitor	$C_a$	780 $\mu$ F		
SSIPT	Switches	$S_{b1}-S_{b4}$	MTP5P06V		
	Diode	$D_{b1}-D_{b4}$	MBR20100CTG		
	Inner diameter	$d_i$	9 mm		
	Coil width	$w$	1.2 mm		
	Outer diameter	$d_o$	88 mm		
	Primary turns	$N_P$	29		
	Secondary turns	$N_S$	30		
	Air gap distance	$g$	45 mm	33 mm	25mm
	Coupling coefficient	$k$	0.1217	0.1739	0.2541
	Primary self inductance	$L_P$	31.48 $\mu$ H	31.477 $\mu$ H	31.467 $\mu$ H
	Secondary self inductance	$L_S$	32.98 $\mu$ H	32.974 $\mu$ H	32.955 $\mu$ H
	Primary winding resistance	$R_{P,w}$	245.8 m $\Omega$	245.76 m $\Omega$	245.59 m $\Omega$
	Secondary winding resistance	$R_{S,w}$	246.3 m $\Omega$	246.32 m $\Omega$	246.33 m $\Omega$
	Compensation capacitance	$C_P$	19.98 nF		
	Compensation capacitance	$C_S$	19.08 nF		
Buck-boost	Switch	$S_c$	IRF540N		
	Diode	$D_c$	MBR20100CTG		
	Capacitor	$C_{c1}$	680 $\mu$ F		
	Inductor	$L_c$	1.2 mH		
	Capacitor	$C_{c2}$	470 $\mu$ F		

studied in this paper, since the magnetic coupler is designed without a magnetic core, the variation of the air gap distance has little effect on the self inductances, as shown in Table II, and no additional control for frequency adaptation is applied. The input voltage  $V_{IN}$  of this prototype is fixed at 50 V. The output voltage  $V_{OUT}$  is maintained at 30 V. A PI controller with  $K_P = 0.01$  and  $K_I = 0.5$  is designed for voltage control.

The SSIPT converter is designed to operate at zero input phase angle. Apart from the winding loss, additional loss to be incorporated into  $R_P$  from the inverter includes conduction loss from  $R_{on}$  and turn-on loss  $P_{switch-on}$  of the MOSFET switches. Additional loss to be incorporated into  $R_S$  includes loss due to the rectifier forward voltage  $V_F$ . Therefore,  $R_P$  and  $R_S$  in (6) are approximated as  $R_P \approx R_{P,w} + 2R_{on} + \frac{16P_{switch-on}}{\pi^2 I_1^2}$  and  $R_S \approx R_{S,w} + \frac{16V_F}{\pi^2 I_2}$ , where  $R_{P,w}$  and  $R_{S,w}$  are the

primary and secondary winding resistances, respectively, of the magnetic coupler.

The efficiency of the SSIPT converter is measured by a Yokogawa PX8000 Precision Power Scope. The buck-boost converter is closed loop controlled and the buck converter is also closed loop controlled with different control references. The efficiency curves of the SSIPT converter versus output power for different values of the voltage ratio are measured as shown in Fig. 8. At  $\frac{V_2}{V_1} = 1$ , near maximum efficiency (with less than 1% error) can be achieved under different loading conditions. Therefore,  $\frac{V_2}{V_1} = 1$  is used as the control reference for achieving maximum efficiency.

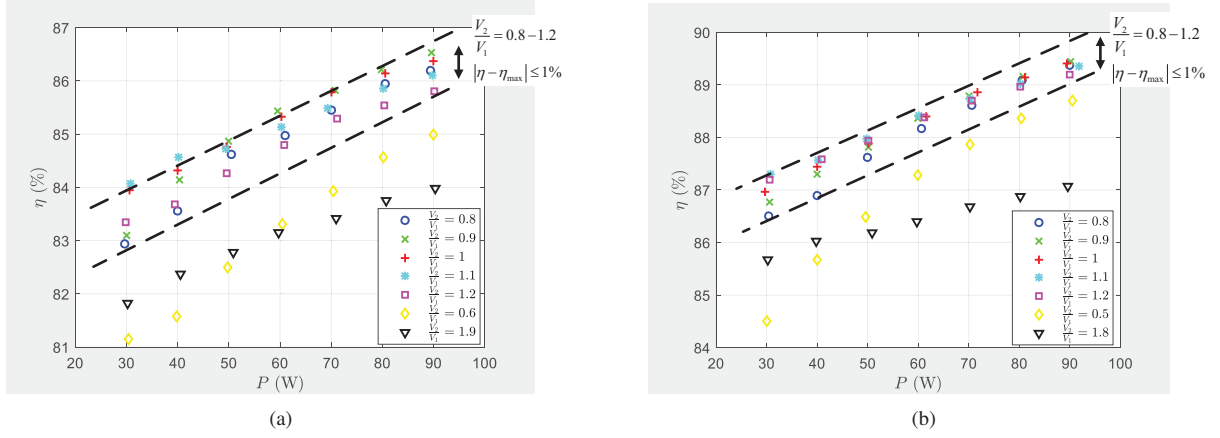


Fig. 8. Measured efficiency of SSIPT converter versus output power under various voltage gains at (a)  $k = 0.1739$ , (b)  $k = 0.2541$ .

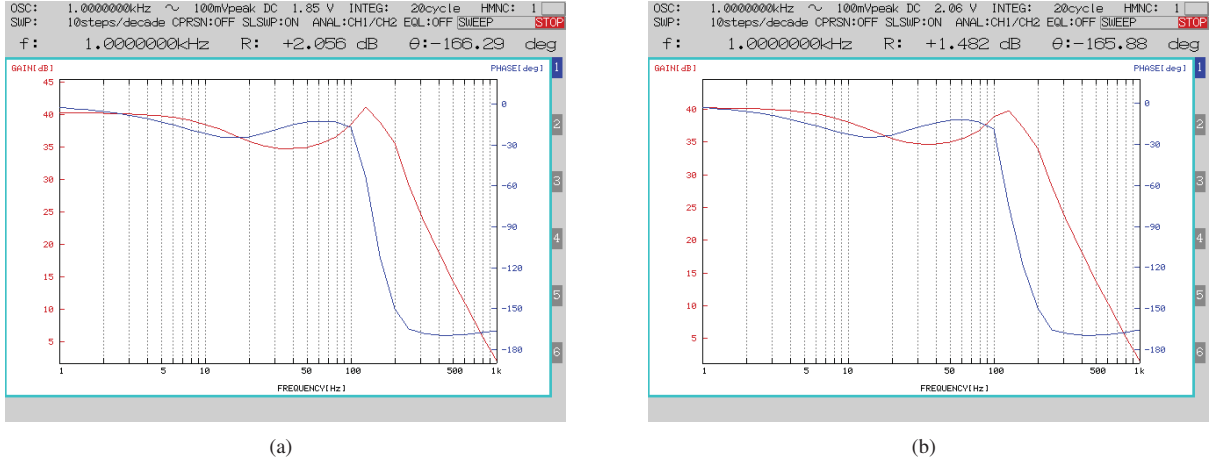


Fig. 9. Measurements of the frequency response of input duty cycle to voltage error of the SSIPT at (a)  $k = 0.1739$ , (b)  $k = 0.2541$ .

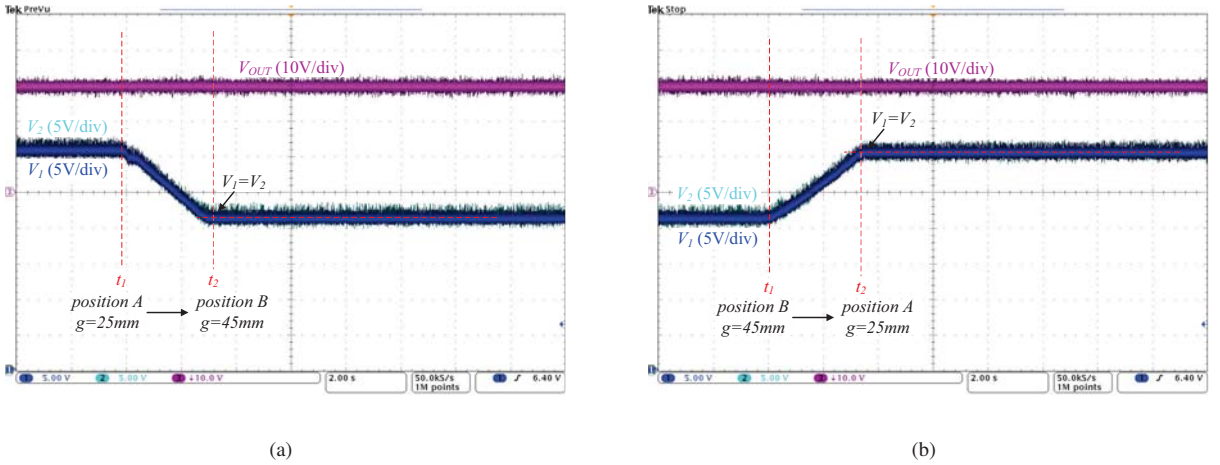


Fig. 10. Transient waveforms of key control parameters of voltage error control with  $g$  dynamically changing (a) from 25 mm to 45 mm, and (b) from 45 mm back to 25 mm. The load resistance  $R$  is 10  $\Omega$ .



### B. Small-Signal Response

Fig. 9 shows the measured frequency response of the input duty cycle to the voltage error of the SS IPT converter. It matches the simulation result shown in Fig. 6(a) and verifies that the design of small-signal parameters of the controller for the cascaded buck-SS IPT converter can follow that of a buck converter.

### C. Transient Response Against Variation of $k$

To show the performance of the proposed control, variation of the air gap distance is introduced by using a dc motor which dynamically varies the position of the secondary side coupler. In Fig. 7, an enlarged image shows the prototype of the loosely coupled transformer with position variation driven by a motor. At position A, the air gap distance  $g$  is 25 mm and the coupling coefficient  $k$  is 0.2541. At position B,  $g$  is 45 mm and the coupling coefficient  $k$  is 0.1217. More parameters of the loosely coupled transformer are shown in Table II.

Experimental waveforms using voltage error control for the dynamical variation of  $g$  at a time scale of 2 s/div are shown in Fig. 10. The efficiency of the system is kept at its optimum by observing that the instantaneous voltages  $V_2$  and  $V_1$  are kept almost identical under variation of  $k$  (or  $g$ ).

As a comparison, experimental waveforms using an implementation of the minimum input current P&O control are also measured as shown in Fig. 11. The same variation speed of  $g$  as in Fig. 10 is used. In the minimum input current P&O control, a perturbation frequency 20 times faster than that adopted in [18] is used with the same perturbation size. Thus, the P&O control in this paper is theoretically faster than that in [18]. Fig. 11 shows that, the instantaneous input current  $I_{IN}$  needs more than 8 second to settle to the steady-state solution. The response of this P&O control is much slower than the voltage error control proposed in this paper against variations of  $k$ .

### D. Transient Response Against Load Variations

Fig. 12 shows the waveforms of voltage tracking processes of the load  $R$  switching from 55  $\Omega$  to 10  $\Omega$  and from 10  $\Omega$  back to 55  $\Omega$ . Using the PI controller, the steady-state error is eliminated. Within 300 ms, the input voltage  $V_1$  and the output voltage  $V_2$  are tracked, so that maximum efficiency of the system are maintained. We have performed experiments using the same parameters based on the P&O control implemented in Section V-C. We found that the transient voltage fluctuations can be harmful to the converters. Therefore, a reduced load range switching from 30 to 10  $\Omega$  is used for comparison of performance between the voltage error control and the P&O control. Four key parameters  $I_{IN}$ ,  $V_1$ ,  $V_2$  and  $V_{OUT}$  of the system as shown in Fig. 3 are chosen for the comparison of waveforms. In Fig. 13, the timebase is set at 4 s/div, the test systems are open loop before  $t_1$  with  $R = 30 \Omega$ , the controls are applied after  $t_1$ , and the loads are switched to  $R = 10 \Omega$  at  $t_2$ .

Fig. 13(a) shows the transient waveforms when the voltage error control is used. It can be observed that  $V_{OUT}$  is always tightly regulated regardless of the excitations applied. This

shows that the independently controlled load-side buck-boost converter can be stable with the input current  $I_2$  (not shown) and voltage  $V_2$  for the whole period of time indicated in Fig. 13(a). As soon as the voltage ratio control is applied at  $t_1$ ,  $\frac{V_2}{V_1}$  is immediately regulated at 1. At the same time,  $I_{IN}$  is also reduced immediately, thus improving the system efficiency. At  $t_2$ , the output power increases by threefold by switching the load resistance from 30  $\Omega$  to 10  $\Omega$ . The voltage ratio is rapidly followed and controlled with  $V_1 = V_2 = 30$  V at steady state.

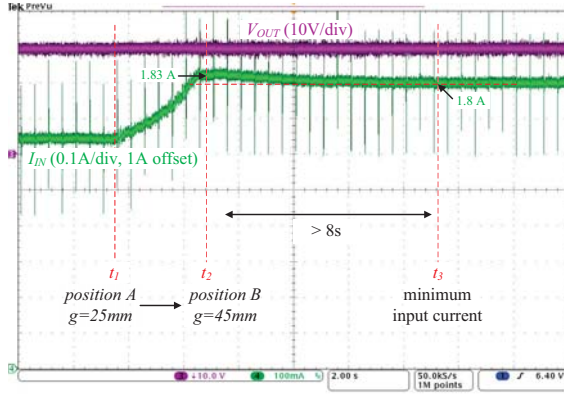
Under the same experimental condition, the minimum input current P&O control produces the transient waveforms shown in Fig. 13(b). The system is completely out of control after  $t_2$  upon load switching. The system instability can be explained as follows. With the same initial condition as that of the voltage ratio control, the minimum input current P&O control is executed right after  $t_1$ . It takes more than 10 seconds to search for the minimum input current. As shown in Fig. 13(b), the voltage ratio  $\frac{V_2}{V_1}$  can be kept between 0.8 and 1.2, which are within the range of maximum efficiency as indicated in Fig. 8. At  $t_2$ , the output power increases three times by switching the load resistance from 30  $\Omega$  to 10  $\Omega$ . The SS IPT converter is a transconductance converter and the load-side converter is a current-driven converter. The output current  $I_2$  of the SS IPT converter is proportional to  $V_1$ . Due to the slow regulation of  $V_1$  by the P&O control,  $I_2$  cannot keep up with the sudden large increment of the output power. However, the control loop of the load-side converter is fast. Therefore, the voltage input  $V_2$  of the current-driven load-side converter rises rapidly trying to acquire more power. As shown in Fig. 13(b),  $V_2$  becomes saturated because of over voltage, leading to the output voltage being out of control. By comparing Figs. 13(a) and 13(b), the voltage error control has better robustness against load-variation due to its faster regulation speed.

### E. Discussion

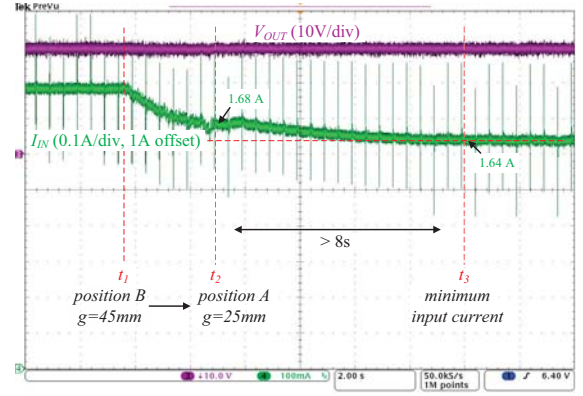
TABLE III  
 $k$ -INDEPENDENT CONVERTER TRANSFER FUNCTION AT MAXIMUM EFFICIENCY

Topology	Converter at maximum efficiency
SS	$\frac{v_o}{v_i} = \sqrt{\frac{R_S}{R_P}}$
PS	$\frac{v_o}{i_i} = \omega L_S \sqrt{\frac{R_S}{R_P}}$

For an IPT converter with a  $k$ -independent input-to-output transfer function and maximum efficiency, the linear control method proposed in this paper can be used. Two example converters are shown in Table III. The voltage input SS-topology is chosen as the example converter of the system. For IPT converters having  $k$ -dependent input-to-output transfer functions and maximum efficiency, before applying this linear control method, the  $k$ -dependent characteristic should be removed by some means, such as using a self-oscillating control as proposed in [26]. Design parameters of the IPT converters are usually known during the design phase. Equivalent series resistances  $R_P$  and  $R_S$  can be estimated from device parameters. The approximated voltage ratio  $\frac{V_2}{V_1}$  can be calculated using (6) as a control reference. Moreover,

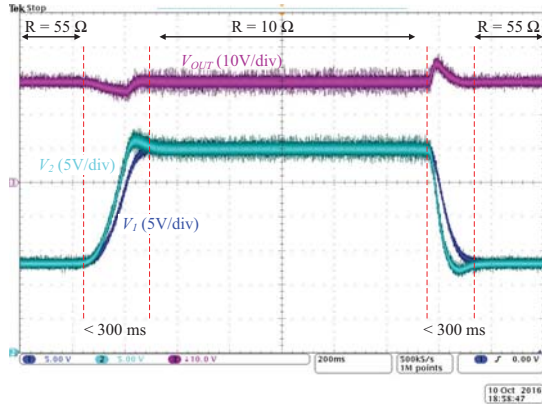


(a)

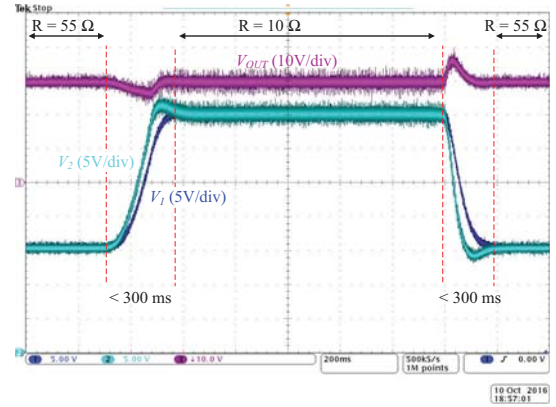


(b)

Fig. 11. Transient waveforms of key control parameters of an implementation of the minimum input current P&O control with  $g$  dynamically changing (a) from 25 mm to 45 mm, and (b) from 45 mm back to 25 mm. The loading condition is  $R = 10 \Omega$ .

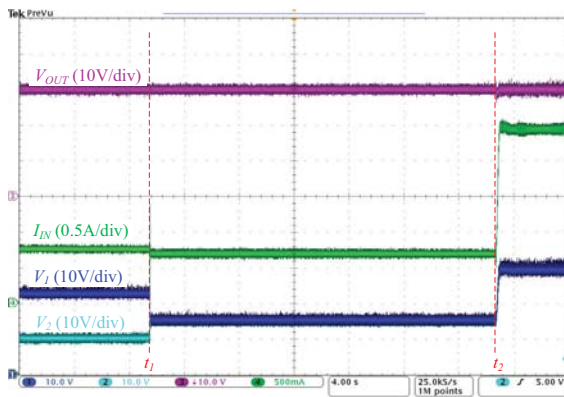


(a)

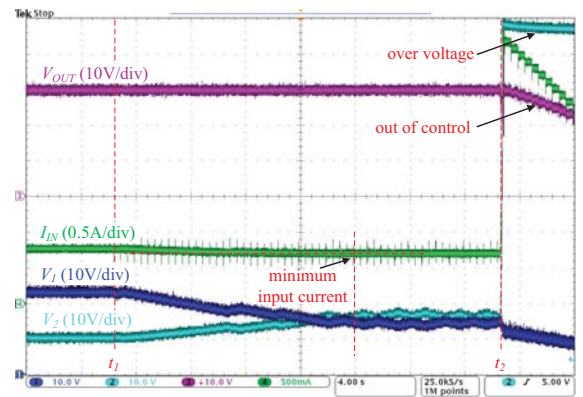


(b)

Fig. 12. Transient waveforms of voltage tracking processes for  $R$  switching from 55  $\Omega$  to 10  $\Omega$  and from 10  $\Omega$  to 55  $\Omega$  at (a)  $k = 0.1739$ , (b)  $k = 0.2541$ .



(a)



(b)

Fig. 13. Transient waveforms of (a) voltage error control, and (b) minimum input current P&O control. At  $t_1$ , the control is executed. At  $t_2$ , load resistance  $R$  is switched from 30  $\Omega$  to 10  $\Omega$ .  $k$  is 0.1739.

if the parameters are not available during the design phase or whenever verification is necessary, they can be measured experimentally as illustrated in Fig. 8. Alternatively, automatic in-circuit measuring methods, such as the P&O method, can also be implemented to determine the voltage ratio  $\frac{V_2}{V_1}$  at maximum efficiency dynamically at the expense of using more sensors. The voltage ratio  $\frac{V_2}{V_1}$  determined can be stored as a control reference for the linear control method proposed in this paper to improve performance.

## VI. CONCLUSION

To achieve maximum efficiency of an inductive power transfer (IPT) system, it is common to use nonlinear perturbation and observation (P&O) control for an IPT system consisting of an IPT converter cascaded with front-side and load-side dc/dc converters. The P&O control is inevitably slow. A linear control scheme is proposed to achieve fast maximum efficiency tracking for an inductive power transfer system in this paper. By observing that the maximum efficiency occurs at a specific input-to-output voltage transfer ratio, a small-signal model for the IPT converter and the front-side converter operating as a combined transconductance converter is developed in this paper. To be compatible with the current output of the transconductance converter, the load-side converter is designed with a stand-alone trans-resistance converter. The controllers for the system are analyzed and experimentally verified to be fast and effective in this paper.

## REFERENCES

- [1] M. Budhia, G. A. Covic, and J. T. Boys, "Design and optimization of circular magnetic structures for lumped inductive power transfer systems," *IEEE Transactions on Power Electronics*, vol. 26, no. 11, pp. 3096–3108, Sept. 2011.
- [2] W. Zhang, J. C. White, A. M. Abraham, and C. C. Mi, "Loosely coupled transformer structure and interoperability study for EV wireless charging systems," *IEEE Transactions on Power Electronics*, vol. 30, no. 11, pp. 6356–6367, Nov. 2015.
- [3] S. Li and C. C. Mi, "Wireless power transfer for electric vehicle applications," *IEEE Journal of Emerging and Selected Topics in Power Electronics*, vol. 3, no. 1, pp. 4–17, March 2015.
- [4] A. P. Sample, D. T. Meyer, and J. R. Smith, "Analysis, experimental results, and range adaptation of magnetically coupled resonators for wireless power transfer," *IEEE Transactions on Industrial Electronics*, vol. 58, no. 2, pp. 544–554, Feb. 2011.
- [5] M. Budhia, J. T. Boys, G. A. Covic, and C. Y. Huang, "Development of a single-sided flux magnetic coupler for electric vehicle IPT charging systems," *IEEE Transactions on Industrial Electronics*, vol. 60, no. 1, pp. 318–328, Jan. 2013.
- [6] R. P. Wojda and M. K. Kazimierzczuk, "Winding resistance of litz-wire and multi-strand inductors," *IET Power Electronics*, vol. 5, no. 2, pp. 257–268, Feb. 2012.
- [7] C. K. Lee, W. X. Zhong, and S. Y. R. Hui, "Effects of magnetic coupling of non-adjacent resonators on wireless power domino-resonator systems," *IEEE Transactions on Power Electronics*, vol. 27, no. 4, pp. 1905–1916, Apr. 2012.
- [8] S. Y. R. Hui, W. Zhong, and C. K. Lee, "A critical review of recent progress in mid-range wireless power transfer," *IEEE Transactions on Power Electronics*, vol. 29, no. 9, pp. 4500–4511, Sept. 2014.
- [9] W. Zhang, S. C. Wong, C. K. Tse, and Q. Chen, "Design for efficiency optimization and voltage controllability of series-series compensated inductive power transfer systems," *IEEE Transactions on Power Electronics*, vol. 29, no. 1, pp. 191–200, Jan. 2014.
- [10] W. Zhang, S. C. Wong, C. K. Tse, and Q. Chen, "Analysis and comparison of secondary series and parallel compensated inductive power transfer systems operating for optimal efficiency and load-independent voltage-transfer ratio," *IEEE Transactions on Power Electronics*, vol. 29, no. 6, pp. 2979–2990, 2014.
- [11] W. Zhang, S. C. Wong, C. K. Tse, and Q. Chen, "Load-independent duality of current and voltage outputs of a series or parallel compensated inductive power transfer converter with optimized efficiency," *IEEE Journal of Emerging and Selected Topics in Power Electronics*, vol. 3, no. 1, pp. 137–146, March 2015.
- [12] X. Qu, H. Han, S. C. Wong, C. K. Tse, and W. Chen, "Hybrid IPT topologies with constant-current or constant-voltage output for battery charging applications," *IEEE Transactions on Power Electronics*, vol. 30, no. 11, pp. 6329–6337, Nov. 2015.
- [13] Z. Huang, S. C. Wong, and C. K. Tse, "Design of a single-stage inductive-power-transfer converter for efficient EV battery charging," *IEEE Transactions on Vehicular Technology*, to appear.
- [14] M. Fu, C. Ma, and X. Zhu, "A cascaded boost-buck converter for high-efficiency wireless power transfer systems," *IEEE Transactions on Industrial Informatics*, vol. 10, no. 3, pp. 1972–1980, Aug. 2014.
- [15] M. Fu, H. Yin, X. Zhu, and C. Ma, "Analysis and tracking of optimal load in wireless power transfer systems," *IEEE Transactions on Power Electronics*, vol. 30, no. 7, pp. 3952–3963, July 2015.
- [16] H. Li, J. Li, K. Wang, W. Chen, and X. Yang, "A maximum efficiency point tracking control scheme for wireless power transfer systems using magnetic resonant coupling," *IEEE Transactions on Power Electronics*, vol. 30, no. 7, pp. 3998–4008, July 2015.
- [17] T. D. Yeo, D. Kwon, S. T. Khang, and J. W. Yu, "Design of maximum efficiency tracking control scheme for closed-loop wireless power charging system employing series resonant tank," *IEEE Transactions on Power Electronics*, vol. 32, no. 1, pp. 471–478, Jan. 2017.
- [18] W. X. Zhong and S. Y. R. Hui, "Maximum energy efficiency tracking for wireless power transfer systems," *IEEE Transactions on Power Electronics*, vol. 30, no. 7, pp. 4025–4034, July 2015.
- [19] S. R. Sander, J. M. Noworolski, X. Z. Liu, and G. C. Verghese, "Generalized averaging method for power conversion circuits," *IEEE Transactions on Power Electronics*, vol. 6, No. 2, pp. 251–259, April 1991.
- [20] S. C. Wong and A. D. Brown, "Analysis, modelling and simulation of series-parallel resonant mode converters," *IEEE Transactions on Power Electronics*, vol. 10, No. 5, pp. 605–614, September 1995.
- [21] A. M. Stankovic, B. C. Lesieutre, and T. Aydin, "Modeling and analysis of single-phase induction machines with dynamic phasors," *IEEE Transactions on Power Systems*, vol. 14, No. 1, pp. 9–14, Feb. 1999.
- [22] A. Emadi, A. Khaligh, C. H. Rivetta, and G. A. Williamson, "Constant power loads and negative impedance instability in automotive systems: definition, modeling, stability, and control of power electronic converters and motor drives," *IEEE Trans. Vehicular Technology*, vol. 55, no. 4, pp. 1112–1125, July 2006.
- [23] R. Ahmadi, D. Paschedag, and M. Ferdowsi, "Closed-loop input and output impedances of DC-DC switching converters operating in voltage and current mode control," in *Proc. IEEE IECON*, Nov. 2010, pp. 2311–2316.
- [24] W. R. Liou, M. L. Yeh, and Y. L. Kuo, "A high efficiency dual-mode buck converter IC for portable applications," *IEEE Transactions on Power Electronics*, vol. 23, no. 2, pp. 667–677, March 2008.
- [25] M. Budhia, G. A. Covic, and J. T. Boys, "Design and optimization of circular magnetic structures for lumped inductive power transfer systems," *IEEE Transactions on Power Electronics*, vol. 26, no. 11, pp. 3096–3108, Nov. 2011.
- [26] L. Xu, Q. Chen, X. Ren, S. C. Wong, and C. K. Tse, "Self-oscillating resonant converter with contactless power transfer and integrated current sensing transformer," *IEEE Transactions on Power Electronics*, to appear.
- [27] M. A. Elizondo, F. K. Tuffner, and K. P. Schneider, "Simulation of inrush dynamics for unbalanced distribution systems using dynamic-phasor models," *IEEE Transactions on Power Electronics*, vol. 32, no. 1, pp. 633–642, Jan. 2017.
- [28] S. Almér, S. Mariéthoz, and M. Morari, "Dynamic phasor model predictive control of switched mode power converters," *IEEE Transactions on Control Systems*, vol. 23, no. 1, pp. 349–356, Jan. 2015.
- [29] G. A. Covic and J. T. Boys, "Modern trends in inductive power transfer for transportation applications," *IEEE Journal of Emerging and Selected Topics in Power Electronics*, vol. 1, no. 1, pp. 28–41, Mar. 2013.
- [30] S. Zhou and C. Chris Mi, "Multi-paralleled LCC reactive power compensation networks and their tuning method for electric vehicle dynamic wireless charging," *IEEE Transactions on Industrial Electronics*, vol. 63, no. 10, pp. 6546–6556, Oct. 2016.
- [31] J. M. Miller, O. C. Onar, C. White, S. Campbell, C. Coomer, L. Seiber, R. Sepe, and A. Steyerl, "Demonstrating dynamic wireless charging of an electric vehicle: the benefit of electrochemical capacitor smoothing," *IEEE Power Electronics Magazine*, vol. 1, no. 1, pp. 12–24, Mar. 2014.



- [32] Q. Chen, S. C. Wong, C. K. Tse, and X. Ruan, "Analysis, design, and control of a transcutaneous power regulator for artificial hearts," *IEEE Transactions on Biomedical Circuits and Systems*, vol. 3, no. 1, pp. 23–31, Feb. 2009.
- [33] S. C. Tang, T. L. T. Lun, Z. Guo, K. W. Kwok, and N. J. McDannold, "Intermediate range wireless power transfer with segmented coil transmitters for implantable heart pumps," *IEEE Transactions on Power Electronics*, vol. 32, no. 5, pp. 3844–3857, May 2017.



**Huang Zhicong** (S'14) received the B.Sc. degree in electrical engineering and automation, in 2010, and M.Sc. degree in mechanical and electronic engineering, in 2013, both from Huazhong University of Science and Technology, Wuhan, China. He is currently working toward the Ph.D. degree in power electronics at the Hong Kong Polytechnic University, Kowloon, Hong Kong.

His current research interests include wireless power transfer and power electronics.



**Chi K. Tse** (M'90–SM'97–F'06) received the BEng (Hons) degree with first class honors in electrical engineering and the PhD degree from the University of Melbourne, Australia, in 1987 and 1991, respectively.

He is presently Chair Professor at the Hong Kong Polytechnic University, Hong Kong, with which he served as Head of the Department of Electronic and Information Engineering from 2005 to 2012. He is author/co-author of 10 books, 20 book chapters and over 500 papers in research journals and conference proceedings, and holds 5 US patents. He was awarded a number of research and industry awards, including Prize Paper Awards by IEEE TRANSACTIONS ON POWER ELECTRONICS in 2001 and 2015, RISP Journal of Signal Processing Best Paper Award in 2014, Best paper Award by International Journal of Circuit Theory and Applications in 2003, two Gold Medals at the International Inventions Exhibition in Geneva in 2009 and 2013, a Silver Medal at the International Invention Innovation Competition in Canada in 2016, and a number of recognitions by the academic and research communities, including honorary professorship by several Chinese and Australian universities, Chang Jiang Scholar Chair Professorship, IEEE Distinguished Lectureship, Distinguished Research Fellowship by the University of Calgary, Gledden Fellowship and International Distinguished Professorship-at-Large by the University of Western Australia. While with the Hong Kong Polytechnic University, he received the President's Award for Outstanding Research Performance twice, Faculty Research Grant Achievement Award twice, Faculty Best Researcher Award, and several teaching awards.

Dr. Tse serves and has served as Editor-in-Chief for the IEEE TRANSACTIONS ON CIRCUITS AND SYSTEMS II (2016-2017), *IEEE Circuits and Systems Magazine* (2012-2015), Editor-in-Chief of *IEEE Circuits and Systems Society Newsletter* (since 2007), Associate Editor for three IEEE Journal/Transactions, Editor for *International Journal of Circuit Theory and Applications*, and is on the editorial boards of a few other journals. He also serves as panel member of Hong Kong Research Grants Council and NSFC, and member of several professional and government committees.



**Siu-Chung Wong** (M'01–SM'09) received the BSc degree in Physics from the University of Hong Kong, Hong Kong, in 1986, the MPhil degree in electronics from the Chinese University of Hong Kong in 1989, and the PhD degree from the University of Southampton, U.K., in 1997.

Dr. Wong joined the Hong Kong Polytechnic in 1988 as an Assistant Lecturer. He is currently an Associate Professor of the Department of Electronic and Information Engineering, The Hong Kong Polytechnic University, where he conducts research in

power electronics. Dr Wong is a senior member of the IEEE and a member of the Electrical College, The Institution of Engineers, Australia. He is an editor of the *Energy and Power Engineering journal* and a member of the Editorial Board of the *Journal of Electrical and Control Engineering*. He serves as a Guest Associate Editor for IEEE JOURNAL OF EMERGING AND SELECTED TOPICS IN POWER ELECTRONICS, Special Issue on Power Electronics for Biomedical Applications, 2014. He serves as an Associate Editor for IEEE TRANSACTIONS ON CIRCUITS AND SYSTEMS II.

From 2012 to 2015, Dr Wong was appointed as a Chutian Scholar Chair Professor by the Hubei Provincial Department of Education, China, and the appointment was hosted by Wuhan University of Science and Technology, Wuhan, China. In 2013, Dr Wong was appointed as Guest Professor by the School of Electrical Engineering, Southeast University, Nanjing, China. He was a visiting scholar at the Center for Power Electronics Systems, Virginia Tech, VA, USA in November 2008, Aero-Power Sci-tech Center, Nanjing University of Aeronautics and Astronautics, Nanjing, China in January 2009, and School of Electrical Engineering, Southeast University, Nanjing, China in March 2012.